Clostridium difficile colonizes alternative nutrient niches during infection across distinct murine gut microbiomes

Authors: Matthew L. Jenior, Jhansi L. Leslie, Vincent B. Young, and Patrick D. Schloss*

Abstract

Clostridium difficile is the largest single cause of hospital-acquired infection in the United States. A major risk factor for *Clostridium difficile* infection (CDI) is prior exposure to antibiotics, as they disrupt the gut bacterial community which protects from *C. difficile* colonization. Multiple antibiotic classes have been associated with CDI susceptibility; many leading to distinct community structures stemming from variation in bacterial targets of action. These microbiomes present separate metabolic challenges to *C. difficile*, therefore we hypothesized that the pathogen adapts its physiology to available nutrients within different gut environments. Utilizing an *in vivo* CDI model, we demonstrated *C. difficile* highly colonized ceca of mice pretreated with any of three antibiotics from distinct classes. Levels of *C. difficile* spore formation and toxin activity varied between animals based on the antibiotic administered. These physiologic processes in *C. difficile* are partially regulated by environmental nutrient concentrations. To investigate metabolic responses of the bacterium *in vivo*, we performed transcriptomic analysis of *C. difficile* from ceca of infected mice across pretreatments. This revealed heterogeneous expression in numerous catabolic pathways for diverse

growth substrates. To assess which resources *C. difficile* exploited, we developed a genome-scale metabolic model with a transcriptomic-enabled metabolite scoring algorithm integrating network architecture. This platform identified nutrients *C. difficile* used preferentially between infections, which were validated through untargeted mass spectrometry of each microbiome. Our results supported the hypothesis that *C. difficile* inhabits alternative nutrient niches across cecal microbiomes with increased preference for nitrogen-containing carbon sources, particularly Stickland fermentation substrates and host-derived aminoglycans.

Importance

Infection by the bacterium *Clostridium difficile* causes an inflammatory diarrheal disease which can become life-threatening, and has grown to be the most prevalent nosocomial infection. Susceptibility to *C. difficile* infection is strongly associated with previous antibiotic treatment, which disrupts the gut microbiota and reduces its ability to prevent colonization. In this study we demonstrated that *C. difficile* altered pathogenesis between hosts pretreated with antibiotics from separate classes, as well as exploited different nutrient sources across these environments. Our metabolite importance calculation also provides a platform to study nutrient requirements of pathogens during the context of infection. Our results suggest that *C. difficile* colonization resistance is mediated by multiple groups of bacteria competing for several subsets of nutrients, and could explain why total reintroduction of competitors through fecal microbial transplant is the most effective treatment to date. This work could ultimately contribute to the identification of targeted measures that prevent or reduce *C. difficile* colonization including pre- and probiotic therapies.

Introduction

Infection by the Gram-positive, spore-forming bacterium *Clostridium difficile* has increased in both prevalence and severity across numerous countries during the last decade (1). In the United States, *C. difficile* was estimated to have caused >500,000 infections and resulted in ~$4.8 billion worth of acute care costs in 2014 (2). *C. difficile* infection (CDI) causes an array of toxin-mediated symptoms ranging from abdominal pain and diarrhea to the more severe conditions pseudomembraneous colitis and toxin megacolon. Prior treatment with antibiotics is the most common risk factor associated with development of CDI (3). Antibiotics likely contribute to susceptibility to CDI by disrupting the gut microbiota (4). In mouse models, multiple antibiotics can induce susceptibility to *C. difficile* colonization (5–7). Notably, each antibiotic resulted in unique gut bacterial communities that were receptive to high levels of *C. difficile* colonization. Others have also shown that antibiotics from multiple classes also alter the gut metabolome, increasing the concentrations of some *C. difficile* growth substrates (6, 8–10). The ability of an unaltered murine gut community to exclude *C. difficile* colonization supports the nutrient-niche hypothesis, which states that an organism must be able to utilize a subset of available resources better than all competitors to colonize the intestine (11, 12). Taken together these results are a strong indication that the healthy gut microbiota inhibits the growth of *C. difficile* by limiting the availability of the substrates it needs to grow.

Based on genomic and *in vitro* growth characteristics, *C. difficile* appears able to adapt to a variety nutrient niches (13). *C. difficile* has a relatively large and mosaic genome, it can utilize a variety of growth substrates, and possesses a diverse array host range (6,

14–16). These qualities are hallmarks of ecological generalists (17). *C. difficile* has also been shown to integrate signals from multiple forms of carbon metabolism to regulate its pathogenesis. *In vitro* transcriptomic analyses suggests that high concentrations of easily metabolized carbon sources, such as glucose or amino acids, inhibit toxin gene expression and sporulation (18, 19). Other studies have indicated that other aspects of *C. difficile* metabolism may be influenced through environmental nutrient concentration-sensitive global transcriptional regulators such as CodY and CcpA (20, 21). These previous analyses have mainly focused on *in vitro* growth (22, 23) or colonization of germfree mice (14, 21). Although these analyses are informative, they are either primarily directed toward the expression of pathogenicity factors or lack the context of the gut microbiota which *C. difficile* must compete against for substrates. Metabolomic investigations have also been used to assay changes in bacterial metabolism as they relate to CDI and have characterized the levels of germinants and growth substrate availability (6, 10); however, metabolomic approaches are unable to attribute a metabolite to specific organisms in the gut community. Thus metabolomics more closely represents the echoes of total community metabolism, not the currently active processes of any one population. It has thus far not been possible to study *C. difficile*'s metabolism *in vivo*.

To overcome these limitations, we implemented transcriptomic and untargeted metabolomic analyses of *C. difficile* and the surrounding environemnt to better understand the active metabolic pathways in a model of infection. Based on the ability of *C. difficile* to grow on a diverse array of carbon sources and its ability to colonize a variety of communities, we hypothesized that *C. difficile* adapts its metabolism to fit the

context of the environment it is attempting colonize. To test this hypothesis, we employed a mouse model of infection to compare the response of *C. difficile* to the gut environment caused by three antibiotics from distinct classes. By characterizing the transcriptome of *C. difficile* in these different communities and the metabolome of the respective environments using paired samples from the same groups of mice, we were able to generate a systems model to directly test the nutrient-niche hypothesis.

Results

Levels of *C. difficile* sporulation and toxin activity vary among different microbiomes. Conventionally-reared SPF mice were treated with either streptomycin, cefoperazone, or clindamycin (Table 1 and Fig. S1). These antibiotics were selected because they each have distinct and significant impacts on the structure of the cecal microbiome (Fig. S2A and S2B). We challenged the antibiotic treated mice and germfree (ex-GF) mice with *C. difficile* stain 630 to understand the pathogen's physiology with and without other microbiota. This toxigenic strain of *C. difficile* was chosen for its moderate clinical severity in mouse models (24) and well-annotated genome (25). After infection, we measured sporulation and toxin production at 18 hours post inoculation. That time point corresponded with when another laboratory strain of *C. difficile* reached its maximum vegetative cell density in the cecum with limited sporulation (26). There was not a significant difference in the number of vegetative *C. difficile* cells in the ceca of mice pretreated with any of the three antibiotics (Fig. 1A). All antibiotic treated and ex-GF mice were colonized to ~1×10^8 colony forming units (cfu) per gram of cecal content, while untreated mice maintained colonization resistance to *C. difficile* (Fig. 1A). Despite having the same number of vegetative *C. difficile* cells, more

spores were detected in ex-GF mice than in the antibiotic pretreated mice (P = 0.003, 0.004, and 0.003; Fig. 1B). There was also a significantly higher toxin titer in ex-GF animals than any other colonized group (all $P < 0.001$), with slight variation between antibiotic pretreatment groups (Fig. 1C). These results showed that *C. difficile* colonized different communities to consistently high levels. In addition, colonization in the context of different microbiomes resulted in moderate differences in the expression of *C. difficile* pathogenicity. To investigate the physiology of *C. difficile* when colonizing distinct susceptible gut environments, we performed whole transcriptome analysis of *C. difficile* from the same cecal content of the same mice.

***C. difficile* alters its gene expression pathways when colonizing distinct antibiotic-pretreated environments.** Utilizing aliquots from the same mice in the previous assays, we attempted to measure differential expression of specific genes associated with *in vivo* phenotype changes reported in previous studies. Microarray-based gene expression measurement was not a viable alternative to sequencing as the amount of background orthologous transcription from other bacterial species would contribute greatly to non-specific binding and bias the true *C. difficile* signal, therefore we employed an RNA-Seq based approach to quantify transcription. As *C. difficile* represented a small percentage of the community in each colonized environment (Fig. S2C), making it impossible to sequence the transcriptome of individual mice due to the depth required to sufficiently sample the transcripts of *C. difficile*. This required the generation of a single transcriptome per condition using pooled mRNA from all mice within each pretreatment group. Following sequencing, read curation, and stringent mapping to *C. difficile* str. 630 genes (Materials & Methods) we implemented two steps

of abundance normalization to compare expression between groups. Transcript abundances for each target gene were first corrected to both read length and target gene length, which resulted in an average per-base expression level for each. Adjusted values were then down-sampled to the same total read abundance for each mapping effort, allowing for even comparison between the conditions. Additionally, before proceeding with the analysis we did and assessed variation in expression of select bacterial housekeeping genes across treatment groups (Fig. S5A). Due to the heterogeneity of *C. difficile* reference genes across strains (27), DNA gyrase subunit A (GyrA), threonyl-tRNA synthetase (ThrS), and ATP-dependent Clp protease (ClpP) were chosen because of their conservation across bacterial phyla and have been commonly utilized as standards of comparison for numerous transcriptional studies (14, 28, 29). Consistent expression for each of the housekeeping genes was observed across treatments, which supported that our results were more likely to be a true reflection of *C. difficile* expression *in vivo*.

Our initial transcriptomic analysis focused on genes involved in sporulation, toxin production, quorum sensing, and metabolite-regulated sigma factors (Fig. S3). Despite large-scale differences between pretreatment groups, no clear trends were evident between gene expression and colonization, sporulation, or toxin production. This further indicated that *C. difficile* adapted its metabolism to the environment that it colonized. As such, we next focused on specific groups of genes known to contribute to *C. difficile* metabolism (Fig. 2A & Table S1). Genes involved in amino acid catabolism, including those that encoded enzymes involved in Stickland fermentation and general peptidases, had the highest level of expression. Stickland fermentation refers to the coupled

159 fermentation of amino acid pairs in which one is deaminated and the other is reduced to
160 ultimately generate ATP (30). This suggested that *C. difficile* catabolized environmental
161 amino acids during infection, regardless of the structure of the surrounding community.
162 Although there were gene categories that were equally expressed across conditions in
163 spite of the community differences, there were patterns of expression for certain gene
164 families and specific genes that were distinct to each antibiotic pretreatment. In mice
165 pretreated with cefoperazone, *C. difficile* tended to have more expression of genes in
166 the ABC sugar transporter and sugar alcohol catabolism (e.g. mannitol) families and
167 fewer genes in the PTS transporter family than the other pretreatment groups. In mice
168 pretreated with clindamycin, *C. difficile* tended to have higher expression of genes from
169 disaccharide catabolism (e.g. beta-galactosidases and trehalose/maltose/cellibiose
170 hydrolases), fermentation product metabolism (including consumption or production of
171 acetate, lactate, butyrate, succinate, ethanol, and butanol), and PTS transporter
172 families. Genes from the sugar alcohol catabolism and ABC sugar transporter families
173 were not highly expressed in the clindamycin-pretreated mice. Finally, in mice
174 pretreated with streptomycin, *C. difficile* had higher levels of expression of genes from
175 the sugar alcohol catabolism (e.g. sorbitol) and PTS transporter families. Combined,
176 these results suggested that while catabolism of amino acids and specific
177 carbohydrates are core components of the *C. difficile* nutritional strategy during
178 infection, *C. difficile* adapted its metabolism across different susceptible environments.

179 **Genome-scale metabolic model structure underscores known *C. difficile***
180 **physiology.** To further investigate which metabolites were differentially utilized between
181 conditions, we created a generalizeable tool to *de novo* generate genome-enabled

182 directed, bipartite metabolic models of bacterial species using KEGG gene and
183 biochemical reaction annotations. We implemented this for *C. difficile* str. 630 shown in
184 Fig. 3A, with enzymes and metabolites were represented by nodes, and their
185 interactions by directed connecting edges. The *C. difficile* str. 630 network we created
186 contained a total of 447 enzymes and 758 metabolites, with 2135 directed edges. To
187 validate our metabolic network, we analyzed network topology by calculating two
188 metrics of centrality, betweenness centrality (BC) and closeness centrality (CC), to
189 determine which nodes are critical to the structure of the metabolic network and if these
190 patterns reflect known biology (Table S2). Both metrics utilize shortest paths, which
191 refer to fewest possible number of network connections that lie between two given
192 nodes. The BC of each node is the fraction of shortest paths that pass through that
193 node and connect all other potential pairs of nodes. In biological terms, this refers to the
194 amount of influence a given hub has on the overall flow of metabolism (31). Similarly,
195 CC is the reciprocal sum of the lengths of shortest paths included in each node's BC.
196 This value demonstrates how essential a given node is to the overall structure of the
197 metabolic network (32). Metabolic network structural studies of *Escherichia coli* have
198 found that metabolites with the highest centrality calculations are involved in
199 fundamental processes in metabolism, namely glycolysis and the citrate acid cycle
200 pathway (33). As such, these metrics allow for assessment of the degree to which a
201 metabolic network accurately depicts established principles of bacterial metabolism.

202 Following application of both methods, we found 5 enzymes that were shared between
203 the top 10 enzymes from BC and CC calculations (2-dehydro-3-
204 deoxyphosphogluconate aldolase, aspartate aminotransferase, pyruvate-flavodoxin

oxidoreductase, formate C-acetyltransferase, and 1-deoxy-D-xylulose-5-phosphate synthase). These enzymes primarily participate in core processes including glycolysis, the pentose phosphate pathway, or the citric acid cycle. Upon analysis of the other 15 high-scoring enzymes combined from BC and CC analyses, the majority were also components of the previously mentioned pathways, as well as several for the metabolism of amino acids (Table S2). Similarly, the intersection of those substrates with high both BC and CC values revealed 6 metabolites as central nodes to the metabolism of *C. difficile* (pyruvate, acetyl-CoA, 2-oxoglutarate, D-4-hydroxy-2-oxoglutarate, D-glyceraldehyde 3-phosphate, and L-glutamate). Not only are these members of glycolysis and the citric acid cycle, but pyruvate, acetyl-CoA, and L-glutamate contribute to numerous intracellular pathways as forms of biological "currency" (33). Notably absent from the most well-connected metabolites were molecules like ATP or NADH. Their exclusion is likely a byproduct of the KEGG LIGAND reference used for network construction, which excludes cofactors from most biochemical reactions. While this may be a limitation of certain analyses, our study was not affected as the primary interest was in those substrates acquired from the environment. These results reflected the defined biological patterns of *C. difficile* and was therefore a viable platform to study metabolism of the pathogen.

Metabolite importance algorithm reveals adaptive nutritional strategies of *C. difficile* during infection of distinct environments. We next sought to include the transcriptomic results into the metabolic model to infer which metabolites *C. difficile* most likely utilized from a given environment. To accomplish this we mapped normalized transcript abundances to the enzyme nodes in the network. Similar

228 approaches have been previously successful in demonstrating that transcript
229 abundance data can be utilized through the lense of genome-scale metabolic networks
230 to accurately predict microbial metabolic responses to environmental pertubation and
231 identify reporter metabolites of changes (34). In our system, the importance of each
232 metabolite was measured as the $\log_2$-transformed difference in average transcript levels
233 of enzymes that use the metabolite as a substrate and those that generate the
234 metabolite as a product (Fig. 3B). A metabolite with a high importance score was more
235 likely obtained from the environment because the expression of genes for enzymes that
236 produce the metabolite were low. It is important to note here that molecules that are
237 more likely produced in our model are not necessarily likely to be released to the
238 environment. Our models do not include the synthesis of large macromolecules (ie. long
239 polypeptides or cytoskeleton) and should therefore only be utilized to consider input
240 metabolites to a network. Due to the previously mentioned limited technical replication
241 of sequencing efforts, we adopted a Monte Carlo-style simulation for iterative random
242 transcriptome comparison to provide statistical validation of our network-based findings.
243 This process generated random score distributions for each metabolite node in the
244 network, which made it possible to calculate a confidence interval that represented
245 random noise for each metabolite. This ultimately allowed for assessment of the
246 probability that a given metabolite was excluded from the associated null distribution
247 (Fig. 3C).

248 To identify the core metabolites that were most essential for *C. difficile* growth,
249 regardless of the environment, we cross-referenced the 40 highest scoring metabolites
250 from each treatment group (Fig. 4A). Aminoglycan N-acetylglucosamine (GlcNAc) was

found to the have the highest median importance of all shared metabolites, which has been shown to be a readily available source of carbon and nitrogen which can be limiting in the gut (21). We went on to confirm that our strain of *C. difficile* could metabolize GlcNAc for growth (Fig. 4B) in *C. difficile* minimal media (35). The Stickland fermentation acceptor proline was also found to be important in all conditions tested (36). *C. difficile* is auxotrophic for not only proline, but also cysteine, leucine, isoleucine, tryptophan, and valine, which prevented testing for *in vitro* growth changes on proline despite providing for modest growth in the no carbohydrate control. Previous analysis of *C. difficile* colonizing GF mice under mono-associated conditions indicated that *C. difficile* uses both sets of metabolites (21); however, use of these metabolites in the context of a complex community of potential competitors has not been observed previously. This analysis indicated that these metabolites might be an integral component of the nutrient niche for *C. difficile*.

***In vivo* metabolomic analysis supports that *C. difficile* consumes metabolites indicated by metabolic modeling.** To further validate the results of our metabolic model, we tested the effect of *C. difficile* on the metabolite pool in additional aliquots of cecal content from the antibiotic-treated and GF mice used in all previous analyses. We employed non-targeted ultra-performance liquid chromatography and mass spectrometry (UPLC-MS) to measure the relative *in vivo* concentrations of metabolites in the conditions investigated, with special attention to those highlighted by large importance scores. We tested whether the susceptible communities had significantly different concentrations of each metabolite relative to untreated SPF mice and whether the presence of *C. difficile* affected the metabolite composition.

First, we compared the relative concentration of important metabolites in untreated SPF mice and antibiotic pretreated mice in the absence of CDI (Fig. 5). We found that the relative concentration of GlcNAc was actually significantly lower in all susceptible conditions (Fig. 5A; all $P < 0.001$). The Stickland fermentation acceptors proline (all $P < 0.05$) and hydroxyproline (all $P < 0.05$) were significantly higher in all susceptible environments tested (Fig. 5B and S7B). Conversely, the Stickland donor alanine was significantly lower across all susceptible conditions (Fig. 5D; all $P < 0.05$). Succinate was significantly higher in both streptomycin and clindamycin pretreated mice (Fig. 5E; all $P < 0.05$). Among the cefoperazone-pretreated SPF and GF mice, we also found that mannitol/sorbitol (Fig. 5C), N-acetylneuraminate (Fig. 5F), and glycine (Fig. S6A) were significantly higher in cefoperazone-treated SPF and GF mice (all $P < 0.05$). These results supported the assertion that antibiotic treatment opened potential nutrient niches that *C. difficile* was able to exploit for its growth.

Second, we compared relative concentrations of important metabolites during CDI and mock-infection within each pretreatment group (Fig. 5). Both groups of host-derived aminoglycans, GlcNAc/GalNAc (Fig. 5A) and Neu5Ac (Fig. 5F), were significantly lower when in the presence of *C. difficile* in ex-GF mice ($P < 0.05$ and 0.01). In agreement with the previous results, we found that the Stickland acceptors proline (Fig. 5B) and hydroxyproline (Fig. S6C) were significantly lower in every *C. difficile* colonized environment (all $P < 0.05$). Glycine, another preferred Stickland acceptor, was lower in each condition following infection with significant change in cefoperazone-pretreated mice (Fig. S6D; $P < 0.05$). The Stickland donors leucine and isoleucine were significantly lower in all infected conditions except streptomycin-pretreated mice (Fig.

297 S6A and S6B; all $P < 0.05$). Concentrations of alanine were also lower in all infected
298 conditions compared to mock infection, however none of the changes met our threshold
299 for significance (Fig. 5D). These results strongly supported the hypothesis that amino
300 acids are a primary energy source of *C. difficile* during infection. A significant difference
301 was seen for mannitol/sorbitol in ex-GF mice ($P < 0.01$), but not in cefoperazone-
302 pretreated mice (Fig. 5C). Although a lower the concentration of succinate in both
303 streptomycin and clindamycin pretreated mice was observed, neither was found to be
304 significant. Overall, metabolomic analysis supported our metabolite importance
305 algorithm for predicting the metabolites utilized by *C. difficile* during different infection
306 conditions. Results from metabolic modeling combined with untargeted metabolomic
307 analysis also suggested a possible hierarchy of preferred growth substrates.

308 ## Discussion

309 Our results expand upon previous understanding of *C. difficile* metabolism during
310 infection by showing that not only does the pathogen adapt its metabolism to life inside
311 of a host (14, 21), but also to the context of the specific gut environment in which it finds
312 itself. Previous transcriptomic efforts to measure the response of *C. difficile* have
313 demonstrated *in vivo* changes in metabolism following colonization of GF mice. In this
314 study, we utilized a conventionally-reared mouse model of infection to compare the
315 response of *C. difficile* to colonization in the context of varied gut communities
316 generated by pretreatment with representatives from distinct classes of antibiotics. With
317 these models, we identified subtle differences in sporulation and toxin activity between
318 each antibiotic-pretreated condition. Transcriptomic sequencing of *C. difficile* across
319 colonized environments indicated complex expression patterns of genes in catabolic

pathways for a variety of carbon sources. Through integration of transcriptomic data with genome-scale metabolic modeling, we were able to deconvolute these signals. This allowed us to observe that *C. difficile* likely genenrated energy by metabolizing specific alternative carbohydrates, carboxylic acids, and aminoglycans across colonized conditions. We also found that Stickland fermentation substrates and products, as well another host-derived amino glycan N-acetylglucosamine, were consistently among the highest scoring shared metabolites which indicated that these metabolites were central to the *in vivo* nutritional strategy of *C. difficile*. To confirm our modeling-based results we employed untargeted mass spectrometry that demonstrated greater availability of many metabolites highlighted by our algorithm in susceptible gut environs. Metabolomic analysis further revealed differential reduction of important metabolites during CDI, which suggested a hierarchy for the utilization of certain growth nutrients.

An explanation for the differences seen in metabolite importance and substrate availability could be the concomitant lower population density of one or more competitors for certain resources. Ex-GF mice, where no other microbial competitors are present, provided a partially controlled system of resource competition. In this condition, Neu5Ac was found to be the most important substrate and concentrations Neu5Ac were significantly higher in susceptible mice. The concentrations of Neu5Ac were concordantly lower in infected mice relative to mock-infected mice. The same trend was also present in cefoperazone-pretreatment, which suggested that *C. difficile* may be less competitive for this host-derived aminoglycan and may only have access when certain competitors are no longer present. In the presence of a microbiota, *C. difficile* population-level nutrient utilization patterns differed across each environment

343 tested. For example, past studies have concluded that specific PTS and ABC transport
344 systems are upregulated *in vivo* (14, 21), but our results indicate more complex
345 regulation with inverse expression of the respective systems between antibiotic
346 pretreatments (Fig. 2). In agreement with earlier research we found that *C. difficile* likely
347 fermented amino acids for energy during infection of GF mice in addition to aminoglycan
348 catabolism. Our results go on to support that this metabolic strategy was conserved
349 across all infection conditions tested. Several Stickland substrates had consistently
350 higher importance scores including alanine, leucine, and proline indeed dropped
351 concentration during infection (Table S3, Fig. 5A, and S6A). Fermentation of amino
352 acids provides not only carbon and energy, but are also a source of nitrogen which is a
353 limited resource in the mammalian lower gastrointestinal tract (37). This makes
354 Stickland fermentation a valuable metabolic strategy, and it stands to reason that *C.*
355 *difficile* would use this strategy across all environments it colonizes. This same principle
356 may also extend to host mucus layer derived aminoglycans as they are another source
357 of carbon and nitrogen which, despite augmented release by members of the microbiota
358 (38), would be present at some basal concentration regardless of other species'
359 intercession. Finally, we did find disagreement in some metabolite importance scores
360 and the difference in *in vivo* concentration of previously suggested *C. difficile* growth
361 substrates between mock infected and infected mice. This may indicate a nutrient
362 preference hierarchy during infection. Based on our results, we propose that amino
363 acids are prized above all other substrates, followed by aminoglycans, then
364 carbohydrates, sugar alcohols, or carboxylic acids depending on their availability in the
365 environment. Since the latter provide carbon and energy, but not nitrogen, it appears

366 that *C. difficile* metabolism strongly values nitrogen-containing carbon sources that fulfill
367 a larger proportion of its biological requirements but this requires additional investigation
368 to confirm.

369 Our systems approach to studying *C. difficile* metabolism during the infection of
370 susceptible communities is novel because it combines multiple levels of biological data
371 to identify metabolic trends that would not be apparent by a single method. Only through
372 integrative multi-omic analysis of *C. difficile* infection employing genomics,
373 transcriptomics, and metabolomics were we able to uncover a much clearer image of *C.*
374 *difficile*'s nutrient niche space during infection in the context of complex microbial
375 communities. By virtue of our importance algorithm's reliance on network topology, the
376 signal contributed by those metabolites on the periphery of the network, which are more
377 likely to be imported from the environment, was amplified. This approach could be
378 especially useful for identifying edges of competition for nutrients between colonizing
379 pathogens and indigenous communties of bacteria, as is the case with *C. difficile*. Our
380 modeling platform may also allow for the identification of emergent properties for the
381 metabolism of *C. difficile* during infection. One example could be the appearance of
382 CO_2, an apparent metabolic end product, in the list of shared important metabolites.
383 Although this may be a shortcoming of the genome annotation, one group has posited
384 that *C. difficile* may actually be autotrophic under certain conditions (39). These findings
385 highlight that our method not only identifies growth substrates, but reports all
386 metabolites that are being utilized for other processes.

387 Several factors limited our ability to generate and interpret transcriptomic and
388 metabolomic data. Most prominently, we were forced to pool the cecal contents of

multiple animals to generate a sufficient quantity of high quality RNA that would permit us to sample the transcriptome of a rare member of the microbiome. Due to possible biological variation between samples that could be masked by this approach, we quantified within-group sample variation for vegetative CFU, 16S rRNA gene abundance, and untargeted mass-spectrometry (Fig. S5B-D). This revealed extremely low variablity in each treatment group at multiple levels of biology, and since these data were collected using matched cecal samples, we were more confident that our transcriptomic results reflected reality. Metabolomic comparisons were also complicated by the fact that multiple organisms contribute to the metabolite pool. The metabolic patterns of the other species in each system (host and microbe) could instead be altered by pathogen colonization. As the concentrations of metabolites in our untargeted assay were reported in relative terms, it was difficult to discern whether the available biomass of *C. difficile* reaches a level to create these differences on its own. Possible limitations of our modeling approach also existed, despite much of our results being consistent with previously published work and our own untargeted metabolomic analysis. Ultimately, the metabolite importance calculation is dependent on correct and existing gene annotation. In this regard it has been shown that the pathway annotations in KEGG are robust to missing elements (40), however this does not completely eliminate the possibility for this type of error. Due to the topology of the metabolic network, we were also unable to integrate stoichiometry for each reaction which may effect rates of consumption or production. Reaction reversibility also varies depending on versions of enzymes possessed by each species. Incorrect directionality annotations may lead to mislabeling reactants or products and potentially lead to incorrect

importance calculations. With additional manual curation of the *C. difficile* metabolic network, more species specific discoveries can eventually be made. Ultimately, the application of multiple methods to study the altered physiology of *C. difficile* in mock-infected and infected communities allowed us to validate our results based on known elements of *C. difficile* biology and to internally cross validate the novel results from our experiments. Ultimately, these results combine to underscore predictions of nutrient niche plasticity.

Our combined genomic, transcriptomic, and metabolomic analysis showed that when infecting diverse host-associated gut environments, *C. difficile* optimized its nutrient utilization profile to each gut environment and effectively colonize the host. Focusing on previously established metabolic capabilities of the pathogen, we identify that these forms of metabolism are differentially important to *C. difficile* when colonizing distinct environments. These results have implications for the development of targeted measures to prevent *C. difficile* colonization through pre- or probiotic therapy. In the future, this systems-level approach could be easily expanded to study the niche landscape of entire communities of bacteria in response to antibiotic perturbation or pathogen colonization.

Materials and Methods

Animal care and antibiotic administration. Six-to-eight week-old GF C57BL/6 mice were obtained from a single breeding colony maintained at the University of Michigan and fed Laboratory Rodent Diet 5001 from LabDiet for all experiments. All animal protocols were approved by the University Committee on Use and Care of Animals at the University of Michigan and carried out in accordance with the approved guidelines.

Specified SPF animals were administered one of three antibiotics; cefoperazone, streptomycin, or clindamycin (Table 1). Cefoperazone (0.5 mg/ml) and streptomycin (5.0 mg/ml) were administered in distilled drinking water *ad libitum* for 5 days with 2 days recovery with untreated distilled drinking water prior to infection. Clindamycin (10 mg/kg) was given via intraperitoneal injection 24 hours before time of infection. Adapted from a previously described model (24).

***C. difficile* infection and necropsy.** All *C. difficile* strain 630 spores were prepared from a single large batch whose concentration was determined a week prior to challenge. On the day of challenge, 1×10^3 *C. difficile* spores were administered to mice via oral gavage in phosphate-buffered saline (PBS) vehicle. Subsequent quantitative plating to enumerate the spores was performed to ensure correct dosage. Mock-infected animals were given an oral gavage of 100 µl PBS at the same time as those mice administered *C. difficile* spores. 18 hours following infection, mice were euthanized by carbon dioxide asphyxiation and necropsied to obtain the cecal contents. Two 100 µl aliquots were immediately flash frozen for later DNA extraction and toxin titer analysis, respectively. A third 100 µl aliquot was quickly transferred to an anaerobic chamber for quantification of *C. difficile* abundance. The remaining content in the ceca (approximately 1 mL) was mixed with 1 mL of sterile PBS in a stainless steel mortar housed in a dry ice and ethanol bath. The cecal contents of 9 mice from 3 cages was pooled into the mortar. Pooling cecal contents was necessary so that there would be a sufficient quantity of high quality rRNA-free RNA for deep sequencing. The pooled content was then finely ground and stored at -80° C for subsequent RNA extraction.

457 ***C. difficile*** **cultivation and quantification.** Cecal samples were weighed and serially
458 diluted under anaerobic conditions (6% H, 20% CO_2, 74% N_2) with anaerobic PBS.
459 Differential plating was performed to quantify both *C. difficile* spores and vegetative cells
460 by plating diluted samples on CCFAE plates (fructose agar plus cycloserine (0.5%),
461 cefoxitin (0.5%), and erythromycin (0.2%)) at 37° C for 24 hours under anaerobic
462 conditions (41). It is important to note that the germination agent taurocholate was
463 omitted from these plates to quantify only vegetative cells. In parallel, undiluted samples
464 were heated at 60° C for 30 minutes to eliminate vegetative cells and leave only spores
465 (42). These samples were serially diluted under anaerobic conditions in anaerobic PBS
466 and plated on CCFAE with taurocholate (10%) at 37° C for 24 hours. Plating was
467 simultaneously done for heated samples on CCFAE to ensure all vegetative cells had
468 been eliminated.

469 ***C. difficile*** **toxin titer assay.** To quantify the titer of toxin in the cecum a Vero cell
470 rounding assay was performed as in (43). Briefly, filtered-sterilized cecal content was
471 serially diluted in PBS and added to Vero cells in a 96-well plate. Plates were blinded
472 and viewed after 24 hour incubation for cell rounding. A more detailed protocol with
473 product information can be found at:
474 https://github.com/SchlossLab/Jenior_Modeling_mSystems_2017/blob/master/protocols
475 /toxin_assay/Verocell_ToxinActivity_Assay.Rmd

476 **16S rRNA gene sequencing and read curation.** DNA was extracted from
477 approximately 50 mg of cecal content from each mouse using the PowerSoil-htp 96
478 Well Soil DNA isolation kit (MO BIO Laboratories) and an epMotion 5075 automated
479 pipetting system (Eppendorf). The V4 region of the bacterial 16S rRNA gene was

amplified using custom barcoded primers and sequenced as described previously using an Illumina MiSeq sequencer (44). All 63 samples were sequenced on a single sequencing run. The 16S rRNA gene sequences were curated using the mothur software package (v1.36), as described previously (44). In short, paired-end reads were merged into contigs, screened for quality, aligned to SILVA 16S rRNA sequence database, and screened for chimeras. Sequences were classified using a naive Bayesian classifier trained against a 16S rRNA gene training set provided by the Ribosomal Database Project (RDP) (45). Curated sequences were clustered into operational taxonomic units (OTUs) using a 97% similarity cutoff with the average neighbor clustering algorithm. The number of sequences in each sample was rarefied to 2,500 per sample to minimize the effects of uneven sampling.

RNA extraction, shotgun library preparation, and sequencing. Pooled, flash-frozen samples were ground with a sterile pestle to a fine powder and scraped into a sterile 50 ml polypropylene conical tube. Samples were stored at -80° C until the time of extraction. Immediately before RNA extraction, 3 ml of lysis buffer (2% SDS, 16 mM EDTA and 200 mM NaCl) contained in a 50 ml polypropylene conical tube was first heated for 5 minutes in a boiling water bath (46). The hot lysis buffer was added to the frozen and ground cecal content. The mixture was boiled with periodic vortexing for another 5 minutes. After boiling, an equal volume of 37° C acid phenol/chloroform was added to the cecal content lysate and incubated at 37° C for 10 minutes with periodic vortexing. The mixture was the centrifuged at 2,500 x g at 4° C for 15 minutes. The aqueous phase was then transferred to a sterile tube and an equal volume of acid phenol/chloroform was added. This mixture was vortexed and centrifuged at 2,500 x g

503 at 4° for 5 minutes. The process was repeated until aqueous phase was clear. The last
504 extraction was performed with chloroform/isoamyl alcohol to remove the acid phenol. An
505 equal volume of isopropanol was added and the extracted nucleic acid was incubated
506 overnight at -20° C. The following day the sample was centrifuged at 12000 x g at 4° C
507 for 45 minutes. The pellet was washed with 0° C 100% ethanol and resuspended in 200
508 µl of RNase-free water. Samples were then treated with 2 µl of Turbo DNase for 30
509 minutes at 37° C. RNA samples were retrieved using the Zymo Quick-RNA MiniPrep.
510 Completion of the DNase reaction was assessed using PCR for the V4 region of the
511 16S rRNA gene for 30 cycles (Kozich, 2013). Quality and integrity of RNA was
512 measured using the Agilent RNA 6000 Nano kit for total prokaryotic RNA. The Ribo-
513 Zero Gold rRNA Removal Kit Epidemiology was then used to deplete 16S and 18S
514 rRNA from the samples. Prior to library construction, quality and integrity as measured
515 again using the Agilent RNA 6000 Pico Kit. Stranded RNA-Seq libraries were made
516 constructed with the TruSeq Total RNA Library Preparation Kit v2. The Agilent DNA
517 High Sensitivity Kit was used to measure concentration and fragment size distribution
518 before sequencing. High-throughput sequencing was performed by the University of
519 Michigan Sequencing Core in Ann Arbor, MI. For all groups, sequencing was repeated
520 across 4 lanes of an Illumina HiSeq 2500 using the 2x50 bp chemistry.

521 **cDNA read curation, mapping, and normalization.** Raw read curation was performed
522 in a two step process. First, residual 5' and 3' Illumina adapter sequences were
523 removed using CutAdapt (47) on a per library basis. Reads were then quality trimmed
524 using Sickle (Joshi, 2011) on the default settings. An average of ~261,000,000 total
525 reads (both paired and orphaned) remained after quality trimming. Mapping was

accomplished using Bowtie2 (48) and the default stringent settings allowing for 0 mismatches again target reference genes. An average of ~6,880,000 reads in sample each mapped to the annotated nucleotide gene sequences of *Clostridioides difficile* 630 from the KEGG: Kyoto Encyclopedia of Genes and Genomes (49). Optical and PCR duplicates were then removed using Picard MarkDuplicates (http://broadinstitute.github.io/picard/), leaving an average of ~167,000 reads per sample for final analysis (Table S5). The remaining mappings were converted to idxstats format using Samtools (50) and the read counts per gene were tabulated. Discordant pair mappings were discarded and counts were then normalized to read length and gene length to give a per base report of gene coverage. Each collection of reads was then subsampled to 90% of the lowest sequence total across the libraries resulting in even quantities of normalized read abundances in each group to be utilized in downstream analysis. This method was chosen as normalization to housekeeping genes would artificially remove their contributions to metabolic flux and reduce the information provided by our metabolite importance calculations within our metabolic modeling approach.

Reaction Annotation & Bipartite Network Construction. The metabolism of *C. difficile* stain 630 was represented as a directed bipartite graph with both enzymes and metabolites as nodes. Briefly, models were semi-automatically constructed using KEGG (2016 edition) ortholog (KO) gene annotations to which transcripts had been mapped. Reactions that each KEGG ortholog mediate were extracted from ko_reaction.list located in /kegg/genes/ko/. KOs that do not mediate simple biochemical reactions (e.g. mediate interactions of macromolecules) were omitted. Metabolites linked to each

549 reaction were retrieved from reaction_mapformula.lst file located in
550 /kegg/ligand/reaction/ from the KEGG release. Those reactions that did not have
551 annotations for the chemical compounds the interact with are discarded. Metabolites
552 were then associated with each enzyme and the directionality and reversibility of each
553 biochemical conversion was also saved. This process was repeated for all enzymes in
554 the given bacterial genome, with each enzyme and metabolite node only appearing
555 once. The resulting data structure was an associative array of enzymes associated with
556 lists of both categories of substrates (input and output), which could then be
557 represented as a bipartite network. The final metabolic network of C. difficile strain 630
558 contained a total of 1205 individual nodes (447 enzymes and 758 substrates) with 2135
559 directed edges. Transcriptomic mapping data was then re-associated with the
560 respective enzyme nodes prior to substrate importance calculations. Betweenness-
561 centrality and overall closeness centralization indices were calculated using the igraph
562 R package found at http://igraph.org/r/.

563 **Metabolite Importance Calculation.** The substrate importance algorithm (Fig. 3a)
564 favors metabolites that are more likely acquired from the environment (not produced
565 within the network), and will award them a higher score (Fig. 4b & 6c). The presumption
566 of our approach was that enzymes that were more highly transcribed were more likely to
567 utilize the substrates they act on due to coupled bacterial transcription and translation. If
568 a compound was more likely to be produced, the more negative the resulting score
569 would be. To calculate the importance of a given metabolite (m), we used rarefied
570 transcript abundances mapped to respective enzyme nodes. This was represented by t_o
571 and t_i to designate if an enzyme created or utilized m. The first step was to calculate the

572 average expression of enzymes for reactions that either created a given metabolite (i) or
573 consumed that metabolite (ii). For each direction, the sum of transcripts for enzymes
574 connecting to a metabolite were divided by the number of contributing edges (e_o or e_i) to
575 normalize for highly connected metabolite nodes. Next the raw metabolite importance
576 score was calculated by subtracting the creation value from the consumption value to
577 weight for metabolites that are likely acquired exogenously. The difference was $\log_2$
578 transformed for comparability between scores of individual metabolites. This resulted in
579 a final value that reflected the likelihood a metabolite was acquired from the
580 environment. Untransformed scores that already equaled to 0 were ignored and
581 negative values were accounted for by transformation of the absolute value then
582 multiplied by -1. These methods have been written into a single python workflow, along
583 with supporting reference files, and is presented as bigSMALL v1.0 (BacterIal Genome-
584 Scale Metabolic models for AppLied reverse ecoLogy) available in a public Github
585 repository at https://github.com/mjenior/bigsmall.

586 **Transcriptome Randomization and Probability Distribution Comparison.** As
587 sequencing replicates of *in vivo* transcriptomes was not feasible, we applied a Monte
588 Carlo style simulation to distinguish calculated metabolite importances due to distinct
589 transcriptional patterns for the environment measured from those metabolites that were
590 constitutively important. We employed a 10,000-fold bootstrapping approach of
591 randomly reassigning transcript abundance for enzyme nodes and recalculating
592 metabolite importances. This approach was chosen over fitting a simulated
593 transcriptome to a negative binomial distribution because it created a more relevant
594 standard of comparison for lower coverage sequencing efforts. Using this method, each

595 substrate node accumulated a random probability distribution of importance scores
596 which were then used to calculate the median and confidence interval to generate a
597 probability for each metabolite importance score to be the result of more than chance.
598 This was a superior approach to switch randomization since the connections of the
599 network itself was created through natural selection and any large-scale alterations
600 would yield biologically uninformative comparisons (51).

601 **Anaerobic *in vitro C. difficile* growth curves.** The carbon-free variation of *C. difficile*
602 Basal Defined Medium (NCMM) was prepared as previously described (6). Individual
603 carbohydrate sources were added at a final concentration of 5 mg/mL and pair-wise
604 carbohydrate combinations were added at 2.5 mg/mL each (5 mg/mL total). A solution
605 of the required amino acids was made separately and added when noted at identical
606 concentrations to the same study. 245 µl of final media mixes were added to a 96-well
607 sterile clear-bottom plate. A rich media growth control was also included, consisting of
608 liquid Brain-Heart Infusion with 0.5% cysteine. All culturing and growth measurement
609 were performed anaerobically in a Coy Type B Vinyl Anaerobic Chamber (3.0% H, 5.0%
610 CO_2, 92.0% N, 0.0% O_2). *C. difficile* str. 630 was grown for 14 hours at 37° C in 3 mL
611 BHI with 0.5% cysteine. Cultures were then centrifuged at 2000 rpm for 5 minutes and
612 resulting pellets were washed twice with sterile, anaerobic phosphate-buffered saline
613 (PBS). Washed pellets were resuspended in 3 mL more PBS and 5 µl of prepped
614 culture was added the each growth well of the plate containing media. The plate was
615 then placed in a Tecan Sunrise plate reader. Plates were incubated for 24 hours at 37°
616 C with automatic optical density readings at 600 nm taken every 30 minutes. OD_{600}
617 values were normalized to readings from wells containing sterile media of the same type

618 at equal time of incubation. Growth rates and other curve metrics were determined by
619 differentiation analysis of the measured OD_{600} over time in R to obtain the slope at each
620 time point.

621 **Quantification of *in vivo* metabolite relative concentrations.** Metabolomic analysis
622 performed by Metabolon (Durham, NC), a brief description of their methods is as
623 follows. All methods utilized a Waters ACQUITY ultra-performance liquid
624 chromatography (UPLC) and a Thermo Scientific Q-Exactive high resolution/accurate
625 mass spectrometer interfaced with a heated electrospray ionization (HESI-II) source
626 and Orbitrap mass analyzer at 35,000 mass resolution. Samples were dried then
627 reconstituted in solvents compatible to each of the four methods. The first, in acidic
628 positive conditions using a C18 column (Waters UPLC BEH C18-2.1x100 mm, 1.7 µm)
629 using water and methanol, containing 0.05% perfluoropentanoic acid (PFPA) and 0.1%
630 formic acid (FA). The second method was identical to the first but was
631 chromatographically optimized for more hydrophobic compounds. The third approach
632 utilized a basic negative ion optimized conditions using a separate dedicated C18
633 column. Basic extracts were gradient eluted from the column using methanol and water,
634 however with 6.5mM Ammonium Bicarbonate at pH 8. Samples were then analyzed via
635 negative ionization following elution from a hydrophilic interaction chromatography
636 column (Waters UPLC BEH Amide 2.1x150 mm, 1.7 µm) using a gradient consisting of
637 water and acetonitrile with 10mM Ammonium Formate, pH 10.8. The MS analysis
638 alternated between MS and data-dependent MS n scans using dynamic exclusion. The
639 scan range varied slighted between methods but covered 70-1000 m/z. Library matches

for each compound were checked for each sample and corrected if necessary. Peaks were quantified using area under the curve.

Statistical methods. All statistical analyses were performed using R (v.3.2.0). Significant differences between community structure of treatment groups from 16S rRNA gene sequencing were determined with AMOVA in the mothur software package. Significant differences of Inv. Simpson diversity, cfu, toxin titer, and metabolite concentrations were determined by Wilcoxon signed-rank test with Benjamini-Hochberg correction. Undetectable points used half the limit of detection for all statistical calculations. Significant differences for growth curves compared to no carbohydrate control (+ amino acids) were calculated using 1-way ANOVA with Benjamini-Hochberg correction.

Funding Information

This work was supported by funding from the National Institutes of Health to PDS (R01GM099514, P30DK034933, U19AI09087, and U01AI124255), VBY (P30DK034933, U19AI09087, and U01AI124255), a Translational Research Education Certificate grant to JLL (MICHR; UL1TR000433), and was partially supported by a predoctoral fellowship from the Cellular Biotechnology Training Program to MLJ (T32GM008353).

Acknowledgements

The authors would like to acknowledge Charles Koumpouras for assistance with DNA extractions and metabolomic sample preparation. We would also like to acknowledge members of the University of Michigan Germfree Mouse Center, University of Michigan Sequencing Core, and Metabolon for their assistance in experimental design, execution,

and data collection. Pooled and quality trimmed transcriptomic read data and experiment metadata are available through the NCBI Sequence Read Archive (SRA; PRJNA354635). Data processing steps for beginning from raw sequence data to the final manuscript are hosted at http://www.github.com/SchlossLab/Jenior_Modeling_mSystems_2017. The authors would additionally like to thank Geoffrey Hannigan Ph.D, Kaitlin Flynn Ph.D, and Nielsen Baxter Ph.D. for their suggestions on manuscript drafts.

Author Affiliations Department of Microbiology and Immunology, University of Michigan, Ann Arbor, Michigan. Matthew L. Jenior, Jhansi L. Leslie, & Patrick D. Schloss Ph.D.

Department of Internal Medicine/Infectious Diseases Division, University of Michigan Medical Center, Ann Arbor, Michigan. Department of Microbiology and Immunology, University of Michigan, Ann Arbor, Michigan. Vincent B. Young M.D. Ph.D.

Author Contributions M.L.J. conceived, designed and performed experiments, analyzed data, and drafted the manuscript. J.L.L. performed experiments, analyzed data, and contributed to the manuscript. V.B.Y. contributed to the manuscript. P.D.S. interpreted data and contributed the manuscript. The authors declare no conflicts of interest.

Corresponding author Correspondence to Patrick D. Schloss

683 **Table 1 | Antibiotics used during *C. difficile* murine infection models.**

Antibiotic	Class	Target	Activity	Administration	Dosage
Cefoperazone	Cephalosporin (3rd generation)	Primarily Gram-positive bacteria, with increased activity against Gram-negative bacteria	Irreversibly crosslink bacterial transpeptidases to peptidoglycan and prevents cell wall synthesis	Drinking water Ad libitum for 5 days, 2 days untreated drinking water prior to infection	0.5 mg/ml drinking water
Streptomycin	Aminoglycoside	Active against most Gram-negative aerobic and facultative anaerobic bacilli	Protein synthesis inhibitor through binding the 30S portion of the 70S ribosomal subunit	Drinking water Ad libitum for 5 days, 2 days untreated drinking water prior to infection	5.0 mg/ml drinking water
Clindamycin	Lincosamide	Primarily active against Gram-positive bacteria, most anaerobic bacteria, and some mycoplasma	Protein synthesis inhibition through binding to the 23s portion of the 50S ribosomal subunit	Intraperitoneal injection 24 hours prior to infection	10 mg/kg body weight

Figure Legends

Figure 1 | Gut environment context affects *C. difficile* sporulation and toxin activity. Quantification of spore cfu and toxin titer from cecal content of infected mice (n = 9 per group). **(A)** Vegetative *C. difficile* cfu per gram of cecal content (P = n.s.). **(B)** *C. difficile* spore cfu per gram of cecal content. **(C)** Toxin titer from cecal content measured by activity in Vero cell rounding assay. Dotted lines denote limits of detection (LOD). Values for undetectable points were imputed as half the LOD for calculation of significant differences. Significance ($P < 0.05$), denoted by single asterisk, was determined with Wilcoxon signed-rank test with Benjamini–Hochberg correction.

Figure 2 | *C. difficile* alters expression metabolic pathways between antibiotic pretreatment models. Each point in the ternary plot represents a unique gene from the annotated genome of *C. difficile* str. 630. Position reflects the ratio of median rarefied transcript abundance for that gene between the three colonized antibiotic pretreatment models. Genes from specific metabolic pathways of interest are labeled and transcription from all other genes are shown in gray. **(A)** Size of highlighted points is relative to the largest transcript abundance among the antibiotic pretreatments for each gene. Categories of metabolism are displayed separately in **(B-I)**. Genes, annotations, and normalized transcript abundances can be found in Table S1. Refer to Fig. S4 for additional figure interpretation.

Figure 3 | *C. difficile* str. 630 genome-enabled bipartite metabolic network architecture and transcriptomic-enabled metabolite importance calculation. (A) Largest component from the bipartite GEM of *C. difficile* str. 630. Enzyme node sizes reflect the levels of detectable transcript from each gene. Importance algorithm

components: (I) average transcription of reactions consuming a metabolite, (II) average transcription of reactions producing a metabolite, and (III) difference of consumption and production. **(B)** The expanded window displays a partial example of D-fructose importance calculation. Values in the red nodes represent normalized transcript reads mapping to enzymes. **(C)** Example 10000-fold Mont-Carlo simulation results corresponding to a significant importance score for **m**.

Figure 4 | Metabolic network analysis reveals differential carbon source utilization by *C. difficile* across infections. Reported metabolites were calculated to have <2.5% probability to be included in the associated random score distribution. Analysis was performed using the 40 highest scoring metabolites from each condition. **(A)** Shared importance represents the median score of metabolites that were consistently important among all infected conditions. Below the conserved patterns, are shown the distinct important metabolites for each group. **(B)** 18 hour *C. difficile* str. 630 *in vitro* growth validating substrates from network analysis. All statistical comparison was performed relative to no carbohydrate control (all $P < 0.001$). Significance was determined with one-way ANOVA with Benjamini–Hochberg correction.

Figure 5 | Untargeted *in vivo* metabolomics support network-based metabolite importance scores and suggest nutrient preference hierarchy. Paired metabolites were quantified simultaneously as the only differ by chirality making differentiation impossible. Black asterisks inside the panels represent significant differences between mock and *C. difficile*-infected groups within separate treatment groups (all $P < 0.05$). Gray asterisks along the top margin of each panel indicate significant difference from

729 untreated SPF mice (all $P < 0.05$). Significance was determined with Wilcoxon signed-

730 rank test with Benjamini–Hochberg correction.

Supplementary Figure 1 | Experimental timelines for mouse model pretreatments and *C. difficile* infection. 9 wild-type C57BL/6 mice across 3 cages were included in each treatment group. **(A)** Streptomycin or **(B)** cefoperazone administered *ad libitum* in drinking water for 5 days with 2 days recovery with untreated drinking water before infection, **(C)** a single clindamycin intraperitoneal injection one day prior to infection, or **(D)** no antibiotic pretreatment (for both SPF control and GF mice). If no antibiotics were administered in the drinking water, mice were given untreated drinking water for the duration of the experiment beginning 7 days prior to infection. At the time of infection, mice were challenged with 1×10^3 *C. difficile* str. 630 spores. Euthanization and necropsy was done 18 hours post-challenge and cecal content was then collected.

Supplementary Figure 2 | Analysis of bacterial community structure resulting from antibiotic treatment. Results from 16S rRNA gene amplicon sequencing from bacterial communities of cecal content in both mock-infected and *C. difficile* 630-infected animals 18 hours post-infection across pretreatment models. **(A)** Non-metric multidimensional scaling (NMDS) ordination based on Theta_{YC} distances for the gut microbiome of all SPF mice used in these experiments (n = 36). All treatment groups are significantly different from each other groups by AMOVA ($P < 0.001$). **(B)** Inverse Simpson diversity for each cecal community from the mice in (A). Cecal communities from mice not treated with any antibiotics are significantly more diverse than any antibiotic-pretreated condition ($P < 0.001$). **(C)** Representation of 16S amplicon reads contributed by *C. difficile* in each sequenced condition compared to the total bacterial community. The percents listed at the top of each group is the proportion of the total

753 community represented by *C. difficile*. Significantly less were for *C. difficile* were
754 detected in each condition ($P < 0.001$).

755 **Supplementary Figure 3 | Select *C. difficile* gene set expression compared**
756 **between treatment group.** Relative abundances of *C. difficile* transcript for specific
757 genes of interest. **(A)** Transcription for select genes from the *C. difficile* sporulation
758 pathway with the greatest variation in expression between the conditions tested. **(B)**
759 Relative abundances of transcript for genes that encode effector proteins from the *C.*
760 *difficile* pathogenicity locus. **(C)** Transcript abundances for genes associated with
761 quorum sensing in *C. difficile*. **(D)** Transcript relative abundance of select sigma factors
762 which expression or activity is influenced by environmental metabolite concentrations.
763 Asterisks (*) indicate genes from which transcript was undetectable.

764 **Supplementary Figure 4 | Additional explanation for Figure 2 interpretation.**
765 Relative abundance of transcription for *C. difficile* 630 genes during infection across the
766 3 antibiotic pretreatment models used during this study. Points that are located closer to
767 a corner are more highly transcribed in the condition associated with that corner
768 compared to the others. As this shows a 3-dimensional data set in 2 dimensions, there
769 is an amount of distortion proximal to each corner. Simply put for points that are nearer
770 to an edge, a greater percentage of their total transcription was contributed by *C.*
771 *difficile* colonizing those mice. **(A)** This point represents the transcription for a gene that
772 is overrepresented in cefoperazone-pretreated mice. **(B)** This point represents a gene in
773 which transcripts are equally detectable in all 3 conditions. **(C)** Transcripts for this gene
774 are only underrepresented in only cefoperazone-pretreated mice, and are equally
775 detectable in clindamycin and streptomycin-pretreated animals.

Supplementary Figure 5 | Levels of within-group variation across datasets generated for this study. (A) Normalized transcript abundance of select housekeeping and central metabolism genes. (I) Housekeeping genes; DNA gyrase subunit A (GyrA), threonyl-tRNA synthetase (ThrS), and ATP-dependent Clp protease (ClpP).(II) Genes in separate metabolic pathways that contribute to input substrate importance; enolase, glycine reductase (GrdA), and D-proline reductase (PrdA). **(B)** Median sample variance for vegetative *C. difficile* cfu from each colonized condition. **(C)** Median and interquartile range of the sample variance of OTU abundances from 16S rRNA gene sequencing, sample variances for each OTU were calculated individually prior to summary statistic calculations. **(D)** Median and interquartile range of the sample variance of Scaled intensities from untargeted metabolomic analysis, sample variances for each metabolite were in the same fashion as with OTU abundances. Data (other than transcriptomic results) was collected from the same nine animals per group were (n = 9).

Supplementary Figure 6 | Change in *in vivo* concentrations of additional Stickland fermentation substrates. Comparison of concentrations for other Stickland fermentation substrates from *C. difficile*-infected and mock-infected mouse cecal content 18 hours post-infection. Labels in the top left corner of each panel indicate whether the amino acid is a Stickland donor or acceptor. Black asterisks inside the panels denote significant differences between mock and *C. difficile*-infected groups within separate treatment groups (all $P < 0.05$). Gray asterisks along the top margin of each panel indicate significant difference from untreated SPF mice (all $P < 0.05$).

Supplementary Table 1 | Specific genes and normalized cDNA read abundances included in analysis reported in Figure 2. Transcript abundances reported in each of

the antibiotic associated columns were first normalized to both sequencing read length and target gene length. Each of the three groups were then even subsampled to an equal total sequences abundance of 13,000 reads to allow for comparability between groups. Additional columns indicate specific gene annotation (gene, pathways, & KEDD_ID) as well as which group each gene belongs for ternary plot (family).

Supplementary Table 2 | Normalized cDNA read abundances, gene annotations, and enzymatic reaction information used for metabolic model building for *C. difficile* str. 630 KEGG orthologs across colonized conditions. All KEGG orthologs included in the *C. difficile* str. 630 KEGG genome annotation (2015) were included in this analysis. Read abundances were normalized as previously outlined to sequencing read length, target gene length, and even total sampling between groups. Also included are individual enzyme annotation for each KEGG ortholog, as well as the associated biochemical reaction information extracted from reaction/reaction_mapformula.lst from KEGG. Together, KEGG ortholog and enzymatic reaction data were used to reconstruct the metabolic network of *C. difficile* str. 630 in presented analyses.

Supplementary Table 3 | Topology metrics for enzyme and metabolite nodes in the *C. difficile* str. 630 metabolic network. Topology analysis of the metabolic network assembled for this study was performed in the absence of transcriptomic data to assess quality of *de novo* assembled network in its reflection of known bacterial metabolism patterns. Enzyme and metabolite node analysis are presented on separate tabs. Centrality metrics and brief explanations are as follows: Degree is the total number of connections for a given node (both incoming and outgoing), Betweenness is the number of shortest paths connecting all other nodes pairs that pass through the node of

interest, and Closeness is the inverse sum of shortest path length that pass through the node of interest. Combined these calculation inform how strongly connected a node is and how vital it is too overall network structure.

Supplementary Table 4 | Metabolites with significant importance scores for *C. difficile* in each colonized condition. Each tab represents those metabolites found to exceed the significance cutoffs for *C. difficile* str. 630 after colonization of each of the respective susceptible states. These threshold were set for each metabolite independently through Monte Carlo simulation as outlined by Figure 3C. A *p*-value of < 0.05 corresponded to a metabolite scoring outside of the 95% confidence interval in the random distribution, and $p < 0.01$ corresponds to those outside the 99% confidence interval. Confidence interval calculations for non-normal distributions were performed as defined by (52).

Supplementary Table 5 | *In vitro* growth analysis for *C. difficile* 630 with carbon sources identified by metabolic network algorithm. Analysis of growth on important carbon sources to identify possible differences in utilization efficiency.

837 ## References

838 1. **Lessa, F. C.**, **C. V. Gould**, and **L. C. McDonald**. 2012. Current status of *Clostridium*
839 *difficile* infection epidemiology. Clinical infectious diseases : an official publication of the
840 Infectious Diseases Society of America **55 Suppl 2**:S65–70.

841 2. **Lessa, F. C.**, **Y. Mu**, **W. M. Bamberg**, **Z. G. Beldavs**, **G. K. Dumyati**, **J. R. Dunn**, **M.**
842 **M. Farley**, **S. M. Holzbauer**, **J. I. Meek**, **E. C. Phipps**, **L. E. Wilson**, **L. G. Winston**, **J.**
843 **a Cohen**, **B. M. Limbago**, **S. K. Fridkin**, **D. N. Gerding**, and **L. C. McDonald**. 2015.
844 Burden of *Clostridium difficile* Infection in the United States. The New England Journal
845 of Medicine **372**:825–834.

846 3. **Leffler, D. A.**, and **J. T. Lamont**. 2015. *Clostridium difficile* Infection. New England
847 Journal of Medicine **372**:1539–1548.

848 4. **Britton, R. A.**, and **V. B. Young**. 2014. Role of the intestinal microbiota in resistance
849 to colonization by *Clostridium difficile*. Gastroenterology **146**:1547–1553.

850 5. **Chen, X.**, **K. Katchar**, **J. D. Goldsmith**, **N. Nanthakumar**, **A. Cheknis**, **D. N.**
851 **Gerding**, and **C. P. Kelly**. 2008. A Mouse Model of *Clostridium difficile*-Associated
852 Disease. Gastroenterology **135**:1984–1992.

853 6. **Theriot, C. M.**, **M. J. Koenigsknecht**, **P. E. C. Jr**, **G. E. Hatton**, **A. M. Nelson**, **B. Li**,
854 **G. B. Huffnagle**, **J. Li**, and **V. B. Young**. 2014. Antibiotic-induced shifts in the mouse
855 gut microbiome and metabolome increase susceptibility to *Clostridium difficile* infection.
856 Nat Commun **3114**.

857 7. **Schubert, A. M.**, **H. Sinani**, and **P. D. Schloss**. 2015. Antibiotic-induced alterations
858 of the murine gut microbiota and subsequent effects on colonization resistance against
859 *Clostridium difficile*. mBio **6**.

860 8. **Antunes, L. C. M.**, **J. Han**, **R. B. R. Ferreira**, **P. Loli**, **C. H. Borchers**, and **B. B.**
861 **Finlay**. 2011. Effect of antibiotic treatment on the intestinal metabolome. Antimicrobial
862 Agents and Chemotherapy **55**:1494–1503.

863 9. **Ferreyra, J. A.**, **K. J. Wu**, **A. J. Hryckowian**, **D. M. Bouley**, **B. C. Weimer**, and **J. L.**
864 **Sonnenburg**. 2014. Gut microbiota-produced succinate promotes *Clostridium difficile*
865 infection after antibiotic treatment or motility disturbance. Cell Host and Microbe
866 **16**:770–777.

867 10. **Jump, R. L. P.**, **A. Polinkovsky**, **K. Hurless**, **B. Sitzlar**, **K. Eckart**, **M. Tomas**, **A.**
868 **Deshpande**, **M. M. Nerandzic**, and **C. J. Donskey**. 2014. Metabolomics analysis
869 identifies intestinal microbiota-derived biomarkers of colonization resistance in
870 clindamycin-treated mice. PLoS ONE **9**.

871 11. **Freter, R.**, **H. Brickner**, **M. Botney**, **D. Cleven**, and **A. Aranki**. 1983. Mechanisms
872 that control bacterial populations in continuous-flow culture models of mouse large
873 intestinal flora. Infection and Immunity **39**:676–685.

874 12. **Wilson, K. H.**, and **F. Perini**. 1988. Role of competition for nutrients in suppression
875 of *Clostridium difficile* by the colonic microflora. Infection and Immunity **56**:2610–2614.

876 13. **Sebaihia, M.**, **B. W. Wren**, **P. Mullany**, **N. F. Fairweather**, **N. Minton**, **R. Stabler**,
877 **N. R. Thomson**, **A. P. Roberts**, **A. M. Cerdeño-Tárraga**, **H. Wang**, **M. T. G. Holden**,
878 **A. Wright**, **C. Churcher**, **M. a Quail**, **S. Baker**, **N. Bason**, **K. Brooks**, **T.**

879 **Chillingworth**, **A. Cronin**, **P. Davis**, **L. Dowd**, **A. Fraser**, **T. Feltwell**, **Z. Hance**, **S.**
880 **Holroyd**, **K. Jagels**, **S. Moule**, **K. Mungall**, **C. Price**, **E. Rabbinowitsch**, **S. Sharp**, **M.**
881 **Simmonds**, **K. Stevens**, **L. Unwin**, **S. Whithead**, **B. Dupuy**, **G. Dougan**, **B. Barrell**,
882 and **J. Parkhill**. 2006. The multidrug-resistant human pathogen *Clostridium difficile* has
883 a highly mobile, mosaic genome. Nature genetics **38**:779–786.

884 14. **Kansau, I.**, **A. Barketi-Klai**, **M. Monot**, **S. Hoys**, **B. Dupuy**, **C. Janoir**, and **A.**
885 **Collignon**. 2016. Deciphering adaptation strategies of the epidemic *Clostridium difficile*
886 027 strain during infection through in vivo transcriptional analysis. PLoS ONE **11**.

887 15. **Songer, J. G.**, and **M. A. Anderson**. 2006. *Clostridium difficile*: An important
888 pathogen of food animals. Anaerobe **12**:1–4.

889 16. **Janvilisri, T.**, **J. Scaria**, **A. D. Thompson**, **A. Nicholson**, **B. M. Limbago**, **L. G.**
890 **Arroyo**, **J. G. Songer**, **Y. T. Gröhn**, and **Y. F. Chang**. 2009. Microarray identification of
891 *Clostridium difficile* core components and divergent regions associated with host origin.
892 Journal of Bacteriology **191**:3881–3891.

893 17. **Gripp, E.**, **D. Hlahla**, **X. Didelot**, **F. Kops**, **S. Maurischat**, **K. Tedin**, **T. Alter**, **L.**
894 **Ellerbroek**, **K. Schreiber**, **D. Schomburg**, **T. Janssen**, **P. Bartholomäus**, **D.**
895 **Hofreuter**, **S. Woltemate**, **M. Uhr**, **B. Brenneke**, **P. Grüning**, **G. Gerlach**, **L. Wieler**, **S.**
896 **Suerbaum**, and **C. Josenhans**. 2011. Closely related *Campylobacter jejuni* strains from
897 different sources reveal a generalist rather than a specialist lifestyle. BMC Genomics
898 **12**:584.

899 18. **Neumann-Schaal, M.**, **J. D. Hofmann**, **S. E. Will**, and **D. Schomburg**. 2015. Time-
900 resolved amino acid uptake of *Clostridium difficile* 630 Delta-erm and concomitant
901 fermentation product and toxin formation. BMC Microbiology 281.

902 19. **Nawrocki, K. L.**, **A. N. Edwards**, **N. Daou**, **L. Bouillaut**, and **S. M. McBride**. 2016.
903 CodY-dependent regulation of sporulation in *Clostridium difficile*. Journal of Bacteriology
904 **198**:2113–2130.

905 20. **Dineen, S. S.**, **S. M. McBride**, and **A. L. Sonenshein**. 2010. Integration of
906 Metabolism and Virulence by *Clostridium difficile* CodY. Journal of Bacteriology
907 **192**:5350–5362.

908 21. **Janoir, C.**, **C. Denève**, **S. Bouttier**, **F. Barbut**, **S. Hoys**, **L. Caleechum**, **D.**
909 **Chapetón-Montes**, **F. C. Pereira**, **A. O. Henriques**, **A. Collignon**, **M. Monot**, and **B.**
910 **Dupuy**. 2013. Adaptive strategies and pathogenesis of *Clostridium difficile* from *in vivo*
911 transcriptomics. Infection and Immunity **81**:3757–3769.

912 22. **Matamouros, S.**, **P. England**, and **B. Dupuy**. 2007. *Clostridium difficile* toxin
913 expression is inhibited by the novel regulator TcdC. Molecular Microbiology **64**:1274–
914 1288.

915 23. **Antunes, A.**, **I. Martin-Verstraete**, and **B. Dupuy**. 2011. CcpA-mediated repression
916 of *Clostridium difficile* toxin gene expression. Molecular Microbiology **79**:882–899.

917 24. **Theriot, C. M.**, **C. C. Koumpouras**, **P. E. Carlson**, **I. I. Bergin**, **D. M. Aronoff**, and
918 **V. B. Young**. 2011. Cefoperazone-treated mice as an experimental platform to assess
919 differential virulence of *Clostridium difficile* strains. Gut microbes **2**:326–334.

920 25. **Monot, M.**, **C. Boursaux-Eude**, **M. Thibonnier**, **D. Vallenet**, **I. Moszer**, **C.**
921 **Medigue**, **I. Martin-Verstraete**, and **B. Dupuy**. 2011. Reannotation of the genome
922 sequence of Clostridium difficile strain 630. Journal of Medical Microbiology **60**:1193–
923 1199.

924 26. **Koenigsknecht, M. J.**, **C. M. Theriot**, **I. L. Bergin**, **C. A. Schumacher**, **P. D.**
925 **Schloss**, and **V. B. Young**. 2015. Dynamics and establishment of *Clostridium difficile*
926 infection in the murine gastrointestinal tract. Infection and Immunity **83**:934–941.

927 27. **Metcalf, D.**, **S. Sharif**, and **J. Weese**. 2010. Evaluation of candidate reference
928 genes in Clostridium difficile for gene expression normalization. Anaerobe **16**:439–443.

929 28. **Gendron, N.**, **H. Putzer**, and **M. Grunberg-Manago**. 1994. Expression of both
930 Bacillus subtilis threonyl-tRNA synthetase genes is autogenously regulated. Journal of
931 Bacteriology **176**:486–494.

932 29. **Sjögren, L.**, and **A. Clarke**. 2011. Assembly of the Chloroplast ATP-Dependent Clp
933 Protease in Arabidopsis Is Regulated by the ClpT Accessory Proteins. The Plant Cell
934 **23**:322–332.

935 30. **Jackson, S.**, **M. Calos**, **A. Myers**, and **W. T. Self**. 2006. Analysis of proline
936 reduction in the nosocomial pathogen *Clostridium difficile*. Journal of Bacteriology
937 **188**:8487–8495.

938 31. **Potapov, A. P.**, **N. Voss**, **N. Sasse**, and **E. Wingender**. 2005. Topology of
939 mammalian transcription networks. Genome informatics. International Conference on
940 Genome Informatics **16**:270–278.

941 32. **Koschutzki, D.**, and **F. Schreiber**. 2008. Centrality analysis methods for biological
942 networks and their application to gene regulatory networks. Gene Regulation and
943 Systems Biology **2008**:193–201.

944 33. **Ma, H. W.**, and **A. P. Zeng**. 2003. The connectivity structure, giant strong
945 component and centrality of metabolic networks. Bioinformatics **19**:1423–1430.

946 34. **Patil, K. R.**, and **J. Nielsen**. 2005. Uncovering transcriptional regulation of
947 metabolism by using metabolic network topology. Proceedings of the National Academy
948 of Sciences of the United States of America **102**:2685–9.

949 35. **Karasawa, T.**, **S. Ikoma**, **K. Yamakawa**, and **S. Nakamura**. 1995. A defined growth
950 medium for Clostridium difficile. Microbiology **141**:371–375.

951 36. **Aboulnaga, H.**, **O. Pinkenburg**, **J. Schiffels**, **A. El-Refai**, **W. Buckel**, and **T.**
952 **Selmer**. 2013. Effect of an oxygen-tolerant bifurcating butyryl coenzyme a
953 dehydrogenase/electron-transferring flavoprotein complex from *Clostridium difficile* on
954 butyrate production in *Escherichia coli*. Journal of Bacteriology **195**:3704–3713.

955 37. **Fuller, M. F.**, and **P. J. Reeds**. 1998. Nitrogen cycling in the gut. Annual review of
956 nutrition **18**:385–411.

957 38. **Marcobal, A.**, **A. M. Southwick**, **K. A. Earle**, and **J. L. Sonnenburg**. 2013. A
958 refined palate: Bacterial consumption of host glycans in the gut. Glycobiology **23**:1038–
959 1046.

960 39. **Köpke, M.**, **M. Straub**, and **P. Dürre**. 2013. *Clostridium difficile* Is an Autotrophic
961 Bacterial Pathogen. PLoS ONE **8**.

962 40. **Green, M. L.**, and **P. D. Karp**. 2006. The outcomes of pathway database
963 computations depend on pathway ontology. Nucleic Acids Research **34**:3687–3697.

964 41. **Wilson, K. H.**, **M. J. Kennedy**, and **F. R. Fekety**. 1982. Use of sodium taurocholate
965 to enhance spore recovery on a medium selective for *Clostridium difficile*. Journal of
966 Clinical Microbiology **15**:443–446.

967 42. **Sorg, J. a.**, and **A. L. Sonenshein**. 2010. Inhibiting the initiation of *Clostridium*
968 *difficile* spore germination using analogs of chenodeoxycholic acid, a bile acid. Journal
969 of Bacteriology **192**:4983–4990.

970 43. **Leslie, J. L.**, **S. Huang**, **J. S. Opp**, **M. S. Nagy**, **M. Kobayashi**, **V. B. Young**, and **J.**
971 **R. Spence**. 2015. Persistence and toxin production by *Clostridium difficile* within human
972 intestinal organoids result in disruption of epithelial paracellular barrier function.
973 Infection and Immunity **83**:138–145.

974 44. **Kozich, J.**, **S. Westcott**, **N. Baxter**, **S. Highlander**, and **P. Schloss**. 2013.
975 Development of a dual-index sequencing strategy and curation pipeline for analyzing
976 amplicon sequence data on the MiSeq Illumina sequencing platform. Appl Environ
977 Microbiol **79**:5112–5120.

978 45. **Wang, Q.**, **G. M. Garrity**, **J. M. Tiedje**, and **J. R. Cole**. 2007. Naive Bayesian
979 classifier for rapid assignment of rRNA sequences into the new bacterial taxonomy.
980 Applied and Environmental Microbiology **73**:5261–5267.

981 46. **Lopez-Medina, E.**, **M. M. Neubauer**, **G. B. Pier**, and **A. Y. Koh**. 2011. RNA
982 isolation of *Pseudomonas aeruginosa* colonizing the murine gastrointestinal tract.
983 Journal of visualized experiments : JoVE 6–9.

984 47. **Martin, M. J.**, **S. Clare**, **D. Goulding**, **A. Faulds-Pain**, **L. Barquist**, **H. P. Browne**,
985 **L. Pettit**, **G. Dougan**, **T. D. Lawley**, and **B. W. Wren**. 2013. The *agr* locus regulates
986 virulence and colonization genes in *Clostridium difficile* 027. Journal of Bacteriology
987 **195**:3672–3681.

988 48. **Langmead, B.**, **C. Trapnell**, **M. Pop**, and **S. L. Salzberg**. 2009. Ultrafast and
989 memory-efficient alignment of short DNA sequences to the human genome. Genome
990 Biol 1–10.

991 49. **Ogata, H.**, **S. Goto**, **K. Sato**, **W. Fujibuchi**, **H. Bono**, and **M. Kanehisa**. 1999.
992 KEGG: Kyoto encyclopedia of genes and genomes. Nucleic Acids Research **27**:29–34.

993 50. **Li, H.**, **B. Handsaker**, **A. Wysoker**, **T. Fennell**, **J. Ruan**, **N. Homer**, **G. Marth**, **G.**
994 **Abecasis**, and **R. Durbin**. 2009. The Sequence Alignment/Map format and SAMtools.
995 Bioinformatics **25**:2078–2079.

996 51. **Basler, G.**, **O. Ebenhöh**, **J. Selbig**, and **Z. Nikoloski**. 2011. Mass-balanced
997 randomization of metabolic networks. Bioinformatics **27**:1397–1403.

998 52. **Bonett, D. G.**, and **R. M. Price**. 2002. Statistical inference for a linear function of
999 medians: confidence intervals, hypothesis testing, and sample size requirements.
1000 Psychological methods **7**:370–383.

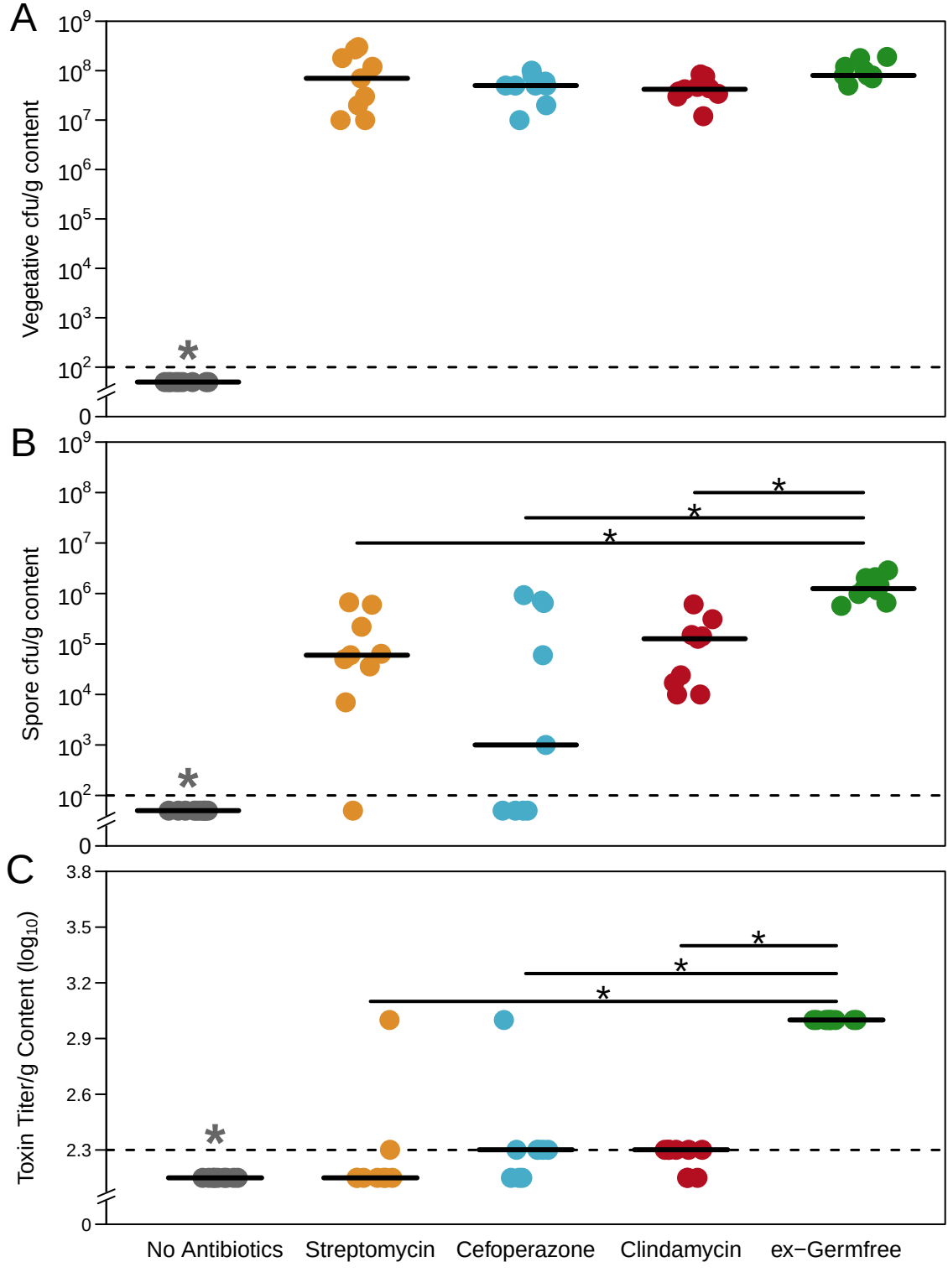
A
Vegetative cfu/g content
10^9
10^8
10^7
10^6
10^5
10^4
10^3
10^2
0
*
B
Spore cfu/g content
10^9
10^8
10^7
10^6
10^5
10^4
10^3
10^2
0
*
*
*
*
C
Toxin Titer/g Content (log_{10})
3.8
3.5
3.2
2.9
2.6
2.3
0
*
*
*
*
No Antibiotics
Streptomycin
Cefoperazone
Clindamycin
ex−Germfree

A

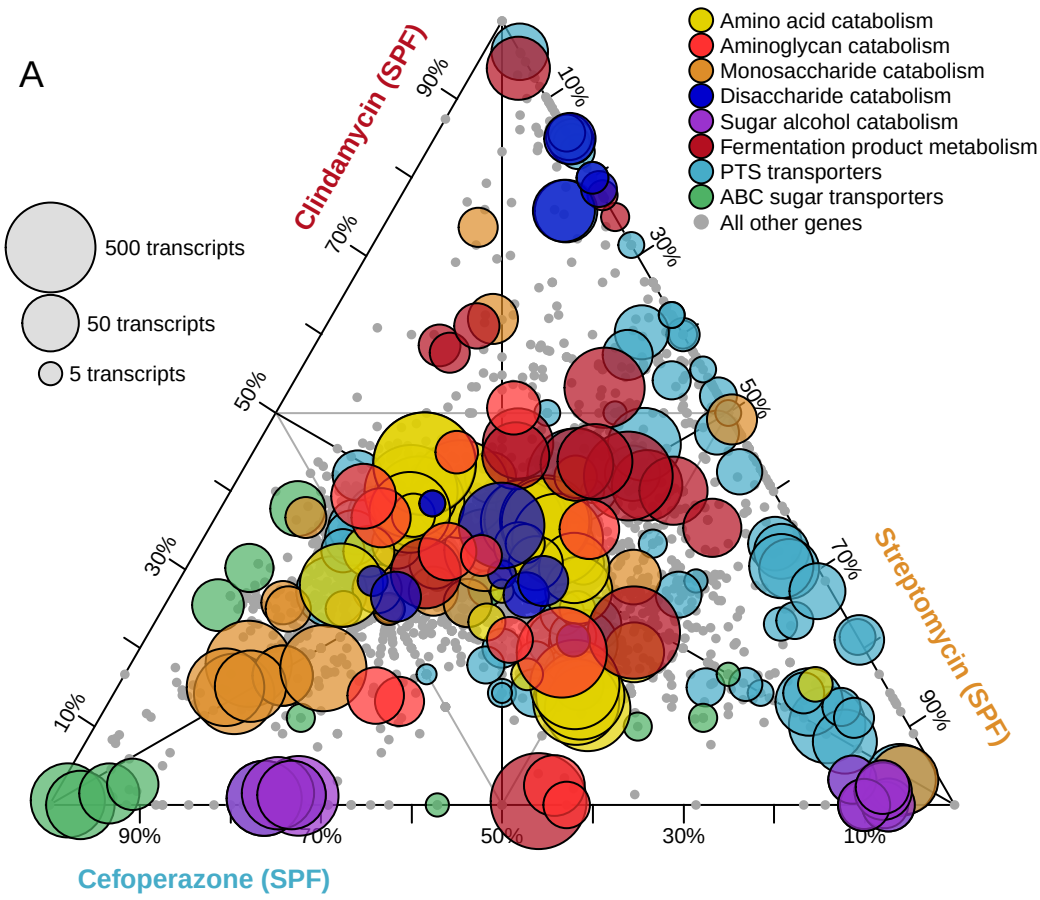

B

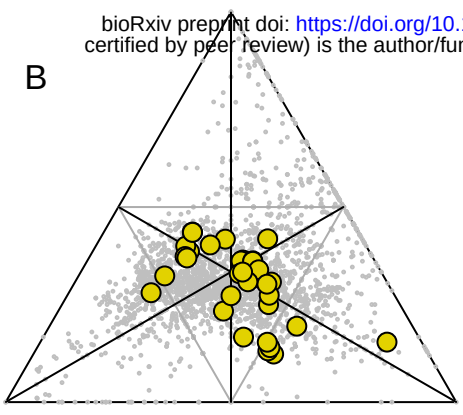

Amino acid catabolism

C

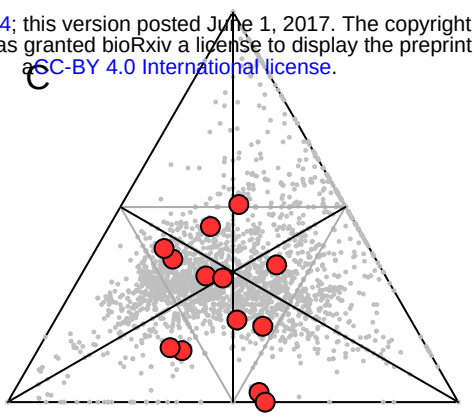

Aminoglycan catabolism

D

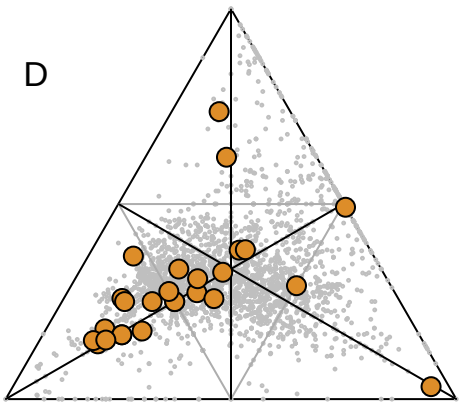

Monosaccharide catabolism

E

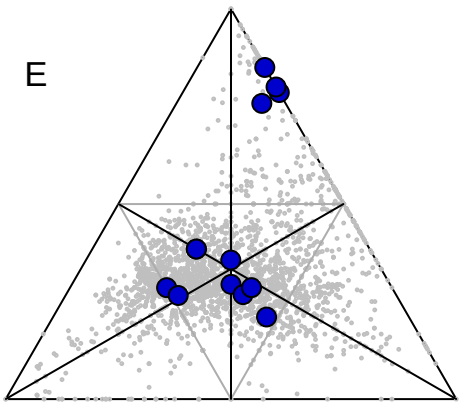

Disaccharide catabolism

F

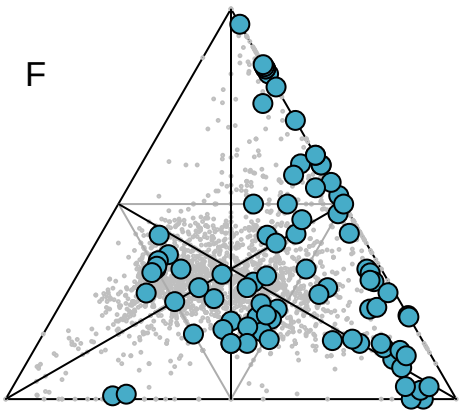

PTS transporters

G

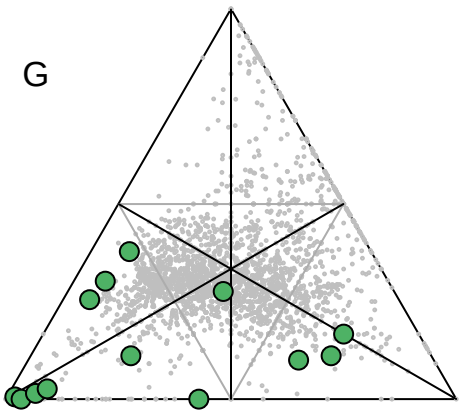

ABC sugar transporters

H

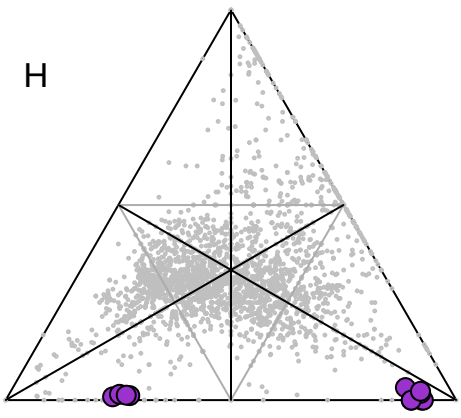

Sugar alcohol catabolism

I

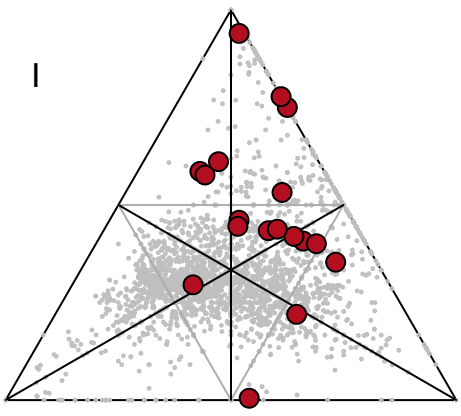

Fermentation product metabolism